Hindawi Publishing Corporation
ISRN Biomaterials
Volume 2013, Article ID 253761, 15 pages
http://dx.doi.org/10.5402/2013/253761

Research Article

Mechanical Properties of Enamel Nanocomposite

Nilormi Biswas,[1] Arjun Dey,[2] Saugata Kundu,[3] Himel Chakraborty,[4] and Anoop K. Mukhopadhyay[1]

[1] *CSIR-Central Glass and Ceramic Research Institute, Kolkata 700032, India*
[2] *Thermal Systems Group, ISRO Satellite Centre, Vimanapura, Bangalore 560 017, India*
[3] *IBM India Pvt. Ltd., Rajarhat, Kolkata 700156, India*
[4] *School of Materials Science and Engineering, Bengal Engineering and Science University, Shibpur, Howrah 711103, India*

Correspondence should be addressed to Anoop K. Mukhopadhyay; anoopmukherjee@cgcri.res.in

Received 10 December 2012; Accepted 9 January 2013

Academic Editors: S. M. Ceré, J. Toppari, and X. Wang

For adult Indian premolar teeth, we report for the first time ever the simultaneous evaluations of nanohardness, Young's modulus, and fracture toughness of the enamel nanocomposite. The nanohardness and Young's moduli were evaluated from near the beginning of the middle enamel region to within ~10 μm of the dentino-enamel junction (DEJ) and in the dentin region using the nanoindentation technique. The fracture toughness from near the middle of the enamel region to near the DEJ zone was measured using the microindentation technique. The deformation was studied using scanning electron microscopy (SEM) and field emission scanning electron microscopy (FESEM). The relative differences in the extents of biomineralization in the enamel and dentin regions were studied by the energy dispersive X-ray (EDS) technique. The variations of the toughness of the enamel as a function of the toughness of the protein matrix phase have been analyzed which showed that the predicted value of the toughness of the protein present in the nanocomposite was comparable to that of other bioproteins reported in the literature. Further, the work of fracture estimated from the measured value of toughness of the enamel nanocomposite agreed well with the experimental data reported in the literature.

1. Introduction

Tooth is a microscopically functionally graded calcium phosphate based natural biocomposite material (Figure 1). Furthermore, tooth has also a hierarchical architecture, for example, from macrostructure to microstructure to nanostructure (Figure 1). The tooth is composed of mainly the hard enamel, the more ductile dentin, and a soft connective tissue, the dental pulp. Enamel is the hardest structure in the human body with approximately 95 wt% hydroxyapatite (HAP). On the other hand, dentine possesses a porous structure and is made up of ~70% inorganic material (i.e., HAP), ~20% organic materials (i.e., collagen fiber), and ~10% water by weight. The enamel microstructure shows different orientations of closely packed enamel prisms or rods. These rods are encapsulated by an organic protein called enamel sheath. Further, the prisms or rods consist of nanosize inorganic HAP crystals with different orientations inside. On the other hand, the dentine has a collagen matrix reinforced with HAP nanocrystal retained as layer by layer. The composite bed of dentine also has dentine tubules and channel-like microstructures which supply the nutrition from the pulp region to the crown part of the teeth. In contrast, the interface between the enamel and dentin junction (DEJ) is arranged with dome-shaped excavations. Therefore, the irregular interface interlocks the two tissues, for example, enamel and dentine. The dentinoenamel nanocomposite junction (DEJ) surface is highly scalloped and has pits into which the shallow depressions of the dentin fit the circular projection of the hard enamel nanocomposite, thus making the enamel nanocomposite cap hold firmly on the dentin [1]. As a result of mastication, the occlusal enamel nanocomposite region and the proximal contact points experience changing loading rates. During high occlusal loading, cracks may be generated in the enamel nanocomposite region, but they rarely propagate across the DEJ into dentin to fracture the entire tooth. The DEJ is

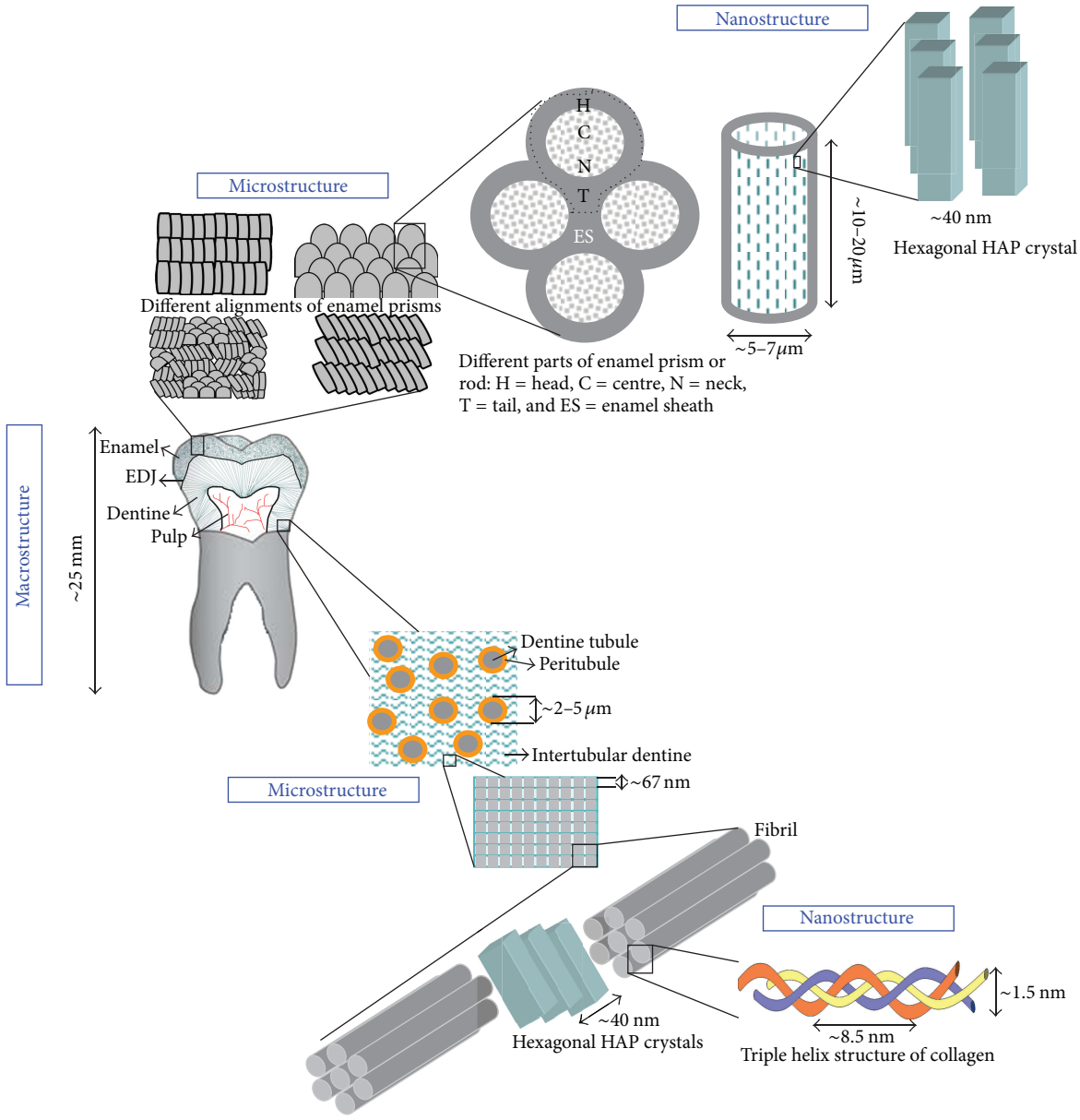

Figure 1: Schematic diagram of the macro-, micro-, and nanostructure of a human tooth enamel and dentin.

reported to be ~75% less tough than dentin and ~5 to 10 times tougher than the enamel nanocomposite [2]. The protein component of the tooth helps in absorbing a large amount of deformation and extra energy dissipation [3]. It is well known that DEJ is a thin layer with properties changing from dentin region to the enamel nanocomposite region. The dentinal fibers terminate into the junction where the HAP crystallites start showing the enamel nanocomposite characteristics [4].

Therefore, considering the huge importance of the DEJ, it is not surprising that many researchers reported nanohardness (H) and Young's modulus (E) of enamel nanocomposite [5–18] wherein occasionally attempts were also made to apply the "Rule of Mixtures" [19–21] to predict Young's modulus data. Typically, the tooth enamel nanocomposite showed nanohardness (H) and Young's modulus (E) in the range of 3 to 5 GPa and 80 to 120 GPa, respectively [5–8, 14, 15]. On the other hand, dentin showed nanohardness (H) and Young's modulus (E) in the range of 0.90 to 1 GPa and 10 to 40 GPa, respectively [5, 9]. The nanoindentation experiments conducted at a constant strain rate of 0.05 s^{-1} gave nanohardness of 5.70–3.60 GPa and Young's modulus of 104–70 GPa across depths of 100–2000 nm in enamel nanocomposite. Microstructure evolution induced by the indenter tip was speculated to be the reason for degradation of the nanomechanical properties at higher depth, for example, 2000 nm. The well-known "Rule of Mixtures" [19–21] was used to obtain the upper and lower bounds of Young's modulus [10].

The finite element model of Spears [11] and the "Rule of Mixtures" was applied by Xie et al. [12] to explain Young's modulus data of enamel nanocomposite. Hypomineralized

enamel was their point of interest. Now, when enamel is hypomineralized, it means that its mineral phase content has been decreased. Therefore, it would be expected as a result that its overall organic phase content will be enhanced in the microstructure. Hence, it was not surprising that these authors [12] had argued that the *higher organic phase content* within the *microstructure* was responsible for an initial lower hardness and elastic modulus of hypomineralized enamel nanocomposite. Young's modulus of enamel nanocomposite was also found to be highly dependent on the contact size during loading. For instance, Young's modulus of hypomineralized enamel nanocomposite varied from about 40–50 GPa to about 70–80 GPa as the contact radius was increased from 0.80 to 6.10 μm.

In comparison, Young's modulus of sound enamel nanocomposite was reported to be a little on the higher side, for example, 60–80 GPa [12]. Recently, the "staggered mineral protein composite model" was also used to predict the shear modulus (G) of the enamel nanocomposite [13]. These authors [13] concluded that, depending on the thickness of the protein matrix layer, the shear modulus of the enamel nanocomposite could vary from as low as 0.5 to as high as 2.6 GPa. Nanoindentation experiments by Rohanizadeh et al. [16] reported Young's moduli of 14.50 and 77.30 GPa and nanohardness of 0.53 and 3.20 GPa, respectively, for hypomineralized and sound enamel nanocomposite of the molar teeth [16]. This information clearly showed that hypomineralized enamel nanocomposite had mechanical properties inferior to those of the sound enamel nanocomposite possibly due to the reasons mentioned by other researchers [12] as mentioned above.

According to He et al. [17], Young's moduli of the top and cross-sectional surface of teeth varied from 60 to 100 and from 40 to 80 GPa, respectively, suggesting that the top surface is stiffer. Using the Tension-shear chain (TSC) model Zhou and Hsiung [18] predicted the average shear modulus of the protein matrix (G_p) of the enamel nanocomposite to be about 0.18 GPa. A strong dependence of G_p on strain rate was also reported.

Similarly, many researchers reported the fracture toughness ($K_{IC(e)}$) of enamel nanocomposite [24, 25, 27, 30, 31, 34, 35, 37–39]. The $K_{IC(e)}$ at DEJ zone was reported to be 0.8 to 0.9 MPa·m$^{0.5}$ [37]. However, $K_{IC(e)}$ varied from 0.70 MPa·m$^{0.5}$ at outer to ~1.30 MPa·m$^{0.5}$ at inner enamel nanocomposite. Further, the direction of fracture was proposed to be dependent on the orientation of the indenter head relative to the *local* enamel nanocomposite structures [24, 25]. White et al. reported $K_{IC(e)}$ of 0.90 and 1.30 MPa·m$^{0.5}$ for parallel and perpendicular loading directions in enamel nanocomposite [27].

For human third molars of young patients, $K_{IC(e)}$ varied from about 0.95 MPa·m$^{0.5}$ at the inner region to about 0.88 MPa·m$^{0.5}$ at the outer enamel nanocomposite region while for the old patients the same varied from about 0.88 MPa·m$^{0.5}$ at the inner to about 0.67 MPa·m$^{0.5}$ at the outer enamel nanocomposite regions [30]. On the other hand, Dong and Ruse [38] reported toughening behavior of human molar teeth using the notch less triangular prism (NTP) specimen $K_{IC(e)}$ test and reported a mean value of 1.50 MPa·m$^{0.5}$. The toughening mechanism of the DEJ zone was explained by the fact that crack paths were deflected as cracks propagated across it.

Bajaj et al. reported [31] that the tooth enamel nanocomposite had a $K_{IC(e)}$ of ~0.90 MPa·m$^{0.5}$. It was noted further that the arrest of cracks in enamel nanocomposite usually occurs while traversing from a less oblique to a more oblique prism orientation and the cracks travelled along the prism boundaries [31]. It has also been proposed that the main toughening mechanisms involved in the enamel nanocomposite were bridging induced by unbroken ligaments of the tissue, crack deflection, microcracking, and ligaments of organic matter bridging the crack [34].

However, recent work by Padmanabhan et al. claimed that $K_{IC(e)}$ of enamel nanocomposite increased with increase in indentation load [35]. Using interfacial fracture mechanics, the $K_{IC(e)}$ of the DEJ region was quantified [39]. It was shown further that prevention of cracks formed in enamel nanocomposite from traversing the interface and causing catastrophic tooth fractures was not necessarily associated with the crack-arrest capabilities of the DEJ itself but rather with the development of crack-tip shielding, primarily from uncracked-ligament bridging, in the mantle dentin region adjacent to the DEJ [39]. DEJ zone thus plays a crucial role for the structural stability of teeth, but the details of how this zone acts as a crack-arrest barrier for flaws formed in the brittle enamel nanocomposite have not been understood fully [22, 23, 26, 28, 29, 32, 33, 36].

A collection of typical literature data [4, 8, 10, 12, 13, 16–18, 22–36, 39] on nanohardness, Young's modulus, and $K_{IC(e)}$ of enamel nanocomposite is presented in Table 1. A critical survey of this data shows that (a) the amount of study on enamel nanocomposite of human premolar teeth is far from significant, (b) most of the data barring a few [30, 34] did not clearly mention from which region, for example, inner, middle, or outer enamel nanocomposite, the data were obtained, (c) very few reports are available [25, 30] where nanohardness, Young's modulus, and $K_{IC(e)}$ were all measured on the same sample, (d) most of the modeling work has concentrated on prediction of Young's modulus of the enamel nanocomposite, and (e) there has not been any significant work on modeling the $K_{IC(e)}$ of the enamel nanocomposite. Therefore, the primary objectives of the present work were (i) to evaluate the nanohardness, Young's modulus, and $K_{IC(e)}$ from near the middle to inner enamel nanocomposite region extending up to the immediate vicinity of DEJ in adult Indian premolar teeth and (ii) to model of the $K_{IC(e)}$ data by using the Reuss model [19], the Voigt model [20], and other approaches. If an appropriate modeling can be developed to predict the $K_{IC(e)}$ of the enamel nanocomposite, then the same could be utilized for making synthetic structures that could possibly mimic the structural performance of the enamel nanocomposite in a more efficient manner.

2. Materials and Methods

In the present study, at least twenty premolar teeth were used, and the average data is reported. All teeth samples

Table 1: A literature survey on nanomechanical and mechanical properties of human teeth.

Human teeth details	Measurement method and load	H (GPa)	E (GPa)	K_{IC} (MPa · m$^{0.5}$) (ND: not determined)	Remarks	K_{IC} modelling (Y/N)	Year/reference number
First molar	Compressive strength		Cusp enamel: 84.1 Side enamel: 77.9	ND	σ_c[a] Cusp enamel: 0.384 GPa σ_c[a] Side enamel: 0.372 GPa	N	1961 [22]
Premolar	3-point bending Strain rate: 0.13 mm/min			ND	Enamel: W_{f1}[a] = 13 J · m^{-2} W_{f2}[a] = 200 J · m^{-2} Dentin: W_{f1}[a] = 550 J · m^{-2} W_{f2}[a] = 270 J · m^{-2}	N	1976 [23]
Two incisors, one molar and one canine	MI[a] P[a] = 300 and 500 gf			Enamel: 0.7–1.27	Direction of fracture is believed to be dependent on the orientation of the indenter head relative to the local enamel structures	N	1981 [24]
Third molars	MMI[a] MI[a] P[a] = 2, 3, 5, 10, 20 and 50 N	Enamel: 3.37 Dentin: 0.57	Enamel: 80 Dentin: 20	Enamel Parallel—1.3 Perpendicular—0.52		N	1998 [25]
Incisor	NI[a] P[a] = 300–2500 μN	Enamel: 4.8 Dentin: 0.8	Enamel: 98 Dentin: 25	ND		N	2000 [26]
Incisor	MI[a] P = 500 gf	Enamel: 3		Enamel Parallel—0.9 Perpendicular—1.3	Amelogenin nanospheres permit crystallite growth in preferred orientations, but ameloblastin inhibit crystallite growth	N	2001 [27]
First molar	NI[a] P[a] = 20 mN	HE[a]: 0.53 SE[a]: 3.2	HE[a]: 14.49 SE[a]: 77.25	ND	Mechanical properties of HE[a] are significantly lower than those of the SE[a]	N	2004 [16]
Third molars	NI[a] $P_{max(p)}$[a]: 1000 μN $P_{max(s)}$[a]: 300 μN	Loading: P_r[a]—4.3 S[a]—1.1 Unloading: P_r[a]—3.9 S[a]—1.4	Loading: P_r[a]—83.4 S[a]—39.5 Unloading: P_r[a]—77.1 S[a]—41.2	ND		N	2005 [8]
Premolar	NI[a] P[a] = 1–450 mN		Enamel TS[a]: 100–60 CS[a]: 80–40	ND	The top surface is stiffer than the cross-section	N	2006 [17]
Molar	CSR[a]: 0.05, 0.005, and 0.0005 s^{-1}			ND	G_p = 0.05–0.23 GPa	Used TSC model to determine E	2006 [18]
Molar enamel	NI[a] CSR[a]: 0.05 s^{-1}	For h_f[a] = 100–2000 nm, H = 5.7–3.6	For h_f[a] = 100–2000 nm, E = 104–70	ND	The decrease in H, E values with depth is speculated to be associated with microstructure evolution that is induced by the indenter tip	Used rule of Mixtures to determine E	2007 [10]

Table 1: Continued.

Human teeth details	Measurement method and load	H (GPa)	E (GPa)	K_{IC} (MPa · m$^{0.5}$) (ND: not determined)	Remarks	K_{IC} modelling (Y/N)	Year/reference number
Premolar	BI[a] and SI[a] P^a = 250 mN	SE[a]: 4.49 DE[a]: 5.01 RE[a]: 4.15 Dry: 4.78 BE[a]: 5.94		ND	HAP nanocrystallites are parallel, diverge from the rod axis by 15–45°, and are at angle of 60° to the central, tail, and edge of the rod, respectively	N	2007 [28]
Molar (hypomineralized) and a sound premolar	NI[a] P^a = 1–500 mN (SE[a]) P^a = 1–200 mN (HE[a])		75–45 as c_r[a] increased from 0.8–6.1 μm E_{sound} = 60–80	ND	Elastic modulus is highly dependent on the contact size during loading	Used FEM[a] of Spears and the rule of mixtures to determine E	2007 [12]
Third molars	NI[a] LR[a]: 1 mN/s P_{max}: 5 mN	H_{young} = 4 H_{old} = 4	E_{young} = 84.4 E_{old} = 91.1	ND		N	2008 [29]
Third molars	MI[a]: P^a = 0.1, 0.25, 0.5, 1, 2, 3, and 5 N. NI[a]: P^a = 5 mN	Young I_e[a] = 3.1 M_e[a] = 3.5 O_e[a] = 4.1 Old I_e[a] = 3 M_e[a] = 3.4 O_e[a] = 4	Young I_e[a] = 75 M_e[a] = 82 O_e[a] = 87 Old I_e[a] = 79 M_e[a] = 90 O_e[a] = 100	Young I_e[a] = 0.95 M_e[a] = 0.88 O_e[a] = 0.88 Old I_e[a] = 0.88 M_e[a] = 0.73 O_e[a] = 0.67	Brittleness (μm^{-1}) Young I_e[a] = 305 M_e[a] = 375 O_e[a] = 393 Old I_e[a] = 313 M_e[a] = 582 O_e[a] = 897	N	2008 [30]
Third molars	Cyclic loading P_{max} = 3–5 N and 1-2 N for HAP			0.9 (3 times that of HAP)	Crack growth occurred primarily along the prism boundaries	N	2008 [31]
Defective premolars, sound premolars	NI[a] $P^a \leq$ 500 mN		E_{perp}: 10.9 G[a]: 2.6	ND	HAP nanocrystals make 33° angle with the loading direction	Used a SMPCS[a] model to determine E	2008 [13]
Third molar	MI[a] P^a = 160 gf	Enamel: 3.5		ND		N	2008 [32]
Third molar	NI[a] with spheroconical tip P^a = 5 and 11 mN		Enamel: 123	ND	I_{st}[a]: 1.6 GPa and I_{sr}[a]: 0.6% at a c_r[a] of 250 nm and a total penetration depth of 7 nm	N	2009 [33]
Third molars	Cyclic loading P_{max} = 3–6 N		O_e = 90 I_e = 70	$K_{c(forward)}$ = 2.11 $K_{c(backward)}$ = 1.17	S_{rt}[a] in the forward direction: 4 J/m^2 S_{rt}[a] in the forward direction: 10 J/m^2	N	2009 [34]
Molar	MI[a] at 0.98, 1.96, 2.94, 4.9, and 9.8 N	3.33, 3.51, 3.22, 3.31 and 3.22		0.85, 0.87, 0.88, 0.94, and 0.98		N	2010 [35]
Incisors	NI[a]: P^a = 500 μN	Enamel rod: head—5.01 tail—4.52 axial sec—4.58	Enamel rod: head—102.56 tail—97.3 axial sec—97.72	ND	μ_e: head—0.087 tail—0.094 axial sec—0.108	N	2011 [36]

Table 1: Continued.

Human teeth details	Measurement method and load	H (GPa)	E (GPa)	K_{IC} (MPa · m$^{0.5}$) (ND: not determined)	Remarks	K_{IC} modelling (Y/N)	Year/reference number
Molars	NI[a] P[a] = 2 mN	E: 7 D: 1	E: 95 D: 19	ND	Cracks in the DEJ travelled along structures with dentin characteristics	N	2011 [4]

[a]CSR: constant strain rate, MMI: modified microindentation, and σ_c: ultimate compressive strength.
W_{f1}: work of fracture for parallel specimen; W_{f2}: work of fracture for perpendicular specimen.
MI: microindentation, NI: nanoindentation, and BI: the Berkovich indentation.
SI: spherical indentation, HE: hypomineralized enamel, SE: sound enamel, DE: dehydrated enamel, RE: rehydrated enamel, BE: burnt enamel, TS: top section, CS: cross-section, and LR: loading rate.
P: applied load; $P_{max(p)}$: maximum load applied for enamel prisms.
$P_{max(s)}$: maximum load applied for enamel sheath, P_r: enamel prism, and S: enamel sheath.
h_f: final depth of penetration, c_r: contact radius, I_e: inner enamel, M_e: middle enamel, O_e: outer enamel, FEM: finite element modeling of Spears, I_{st}: indentation stress, and I_{sr}: indentation strain,
μ_e: coefficient of friction of enamel rod; G: shear modulus of enamel nanocomposite.
S_{rt}: strain energy release rate; SMPCS: staggered mineral-protein composite structure model.
G_p: shear modulus of enamel protein matrix.

were freshly extracted from Indian male patients within the age group of about 62–68 years such that the average age was about 65 years. Only those teeth were chosen which were devoid of any cavity. Visual inspection was made to make sure that surface cracks were also absent. The conventional technique of gamma radiation was used to sterilize the samples. Subsequently they were preserved at 4°C in deionized water. Next, the samples were sectioned in dry condition along the longitudinal direction by a slow speed diamond saw (Minitom, Struers, Denmark). This step was followed by ultrasonic cleaning (Microclean-109, Oscar Ultrasonics, Mumbai, India) using sequentially analytical reagent grade acetone, ethanol, and deionised water. A sectioned half of each sample was then mounted in an epoxy resin. A cold-cure type epoxy was used. Just immediately prior to microstructural and nanomechanical characterizations, the cleaned teeth samples were subsequently polished with diamond pastes (Eastern Diamond Pvt. Ltd., Kolkata, India) starting from 9 μm down to 0.25 μm grit size. At the end of each polishing step, the samples were ultrasonically cleaned in distilled water. This step was necessary to remove the presence of any polishing pastes that could have remained as a smeared layer on the sample surface. The average surface roughness (R_a) resulting from the preparation was characterized after polishing using scanning probe microscopy (SPM) in contact mode. The surface roughness was measured over a single selected area of 50 × 50 μm^2 in Selected specimens and was found to be 0.02 μm. The microstructural characterizations were carried out by optical microscopy (GX51, Olympus, USA) and scanning electron microscopy (SEM, Hitachi S-3400N, Japan). Further, compositional analysis was done with energy dispersive X-ray (EDS) technique by the same SEM machine described earlier. Prior to insertion in the sample chamber for electron microscopy, a 50–70 nm gold coating was deposited on the teeth samples by the arc deposition technique to avoid charging.

The nanoindentation experiments were carried out on the freshly polished samples using a commercial nanoindenter (Fischerscope H100-XYp; Fischer, Switzerland) equipped with a Berkovich tip. The machine worked according to DIN 50359-1 standard. The depth and force sensing resolutions of the machine were 1 nm and 0.20 μN, respectively. The machine was calibrated with nanoindentation based independent evaluation of $H \sim 4.14$ GPa and $E \sim 84.6$ GPa of a Schott BK7 Glass (Schott, Germany). The experiments were conducted at a constant load of 100 mN. Both loading and unloading times were kept fixed at 30 seconds. The Berkovich indenter had a tip radius of about 150 nm and a semiapex angle of 65.3°. The nanohardness (H) and Young's moduli (E) data were evaluated from the load versus depth of penetration plots using the well-established Oliver and Pharr (O-P) method [40]. Two sets of 5 × 5 arrays of indentations were done on the teeth samples. Of these two arrays, one array was located at dentin portion while the other was located covering from near the middle to inner enamel nanocomposite region extending up to the immediate vicinity (e.g., within ~10 μm) of the DEJ region. During all the nanoindentation experiments, the ambient temperature was kept at 30°C and the relative humidity was ~70%.

In addition, the $K_{IC(e)}$ data were evaluated from near the middle to inner enamel nanocomposite region extending up to the immediate vicinity of DEJ at a load of 4.9 N by using the measurements of the surface crack lengths emanated from four corners of a standard Vickers diamond square pyramidal indenter fitted in a hardness tester (Leco HV700, USA). Further, indentations were also made under similar experimental condition as above in the dentin region near the DEJ zone with a view to generate a comparative picture of the deformation and/or damage patterns in the three regions of teeth as discussed above. The following relationship was used for evaluation of the $K_{IC(e)}$ values [41]:

$$K_{IC(e)} = 0.016\left(\frac{E}{H}\right)^{0.5}\left(\frac{P}{D^{1.5}}\right), \quad (1)$$

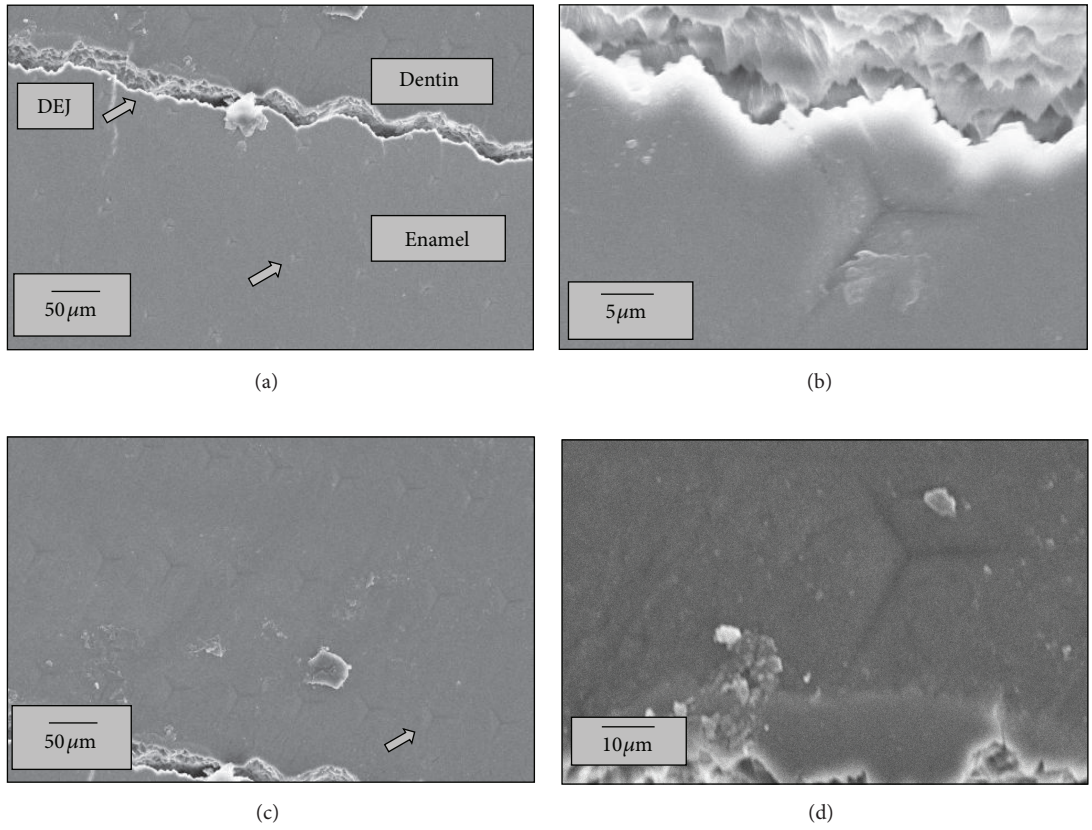

Figure 2: Typical SEM photomicrographs of (a) nanoindentation array in the enamel nanocomposite zone near the DEJ zone, (b) a single indent at the enamel nanocomposite zone near the DEJ zone, (c) nanoindentation array in the dentin zone, and (d) a single indent at the dentin zone near the DEJ zone.

where 0.016 is a constant factor which is related to geometry of the indenter and calibration data, E is Young's modulus of the enamel nanocomposite measured independently by the nanoindentation technique as mentioned above, H is hardness of the enamel nanocomposite measured at a macroscopic load P (=4.9 N), and D is the characteristic crack length that is composed of half the average indentation diagonal plus the average crack length measured from the tip of indentation impression up to the crack tip created at the load P.

3. Results

The lower and higher magnification SEM photomicrographs of the array of the [nanoindents] in the enamel nanocomposite and dentin portions around the DEJ zone are shown in Figures 2(a), 2(c), 2(b), and 2(d), respectively. These photomicrographs do not show any obvious sign of cracking. The load (P) versus nanoindentation depth (h) plots (Figure 3) confirmed that a much higher amount of energy was absorbed during deformation at the nanoscale by the dentin than by the enamel nanocomposite. Both the nanohardness (H), Figure 4(a), and Young's moduli (E), Figure 4(b), of enamel nanocomposite were much higher than those of dentin

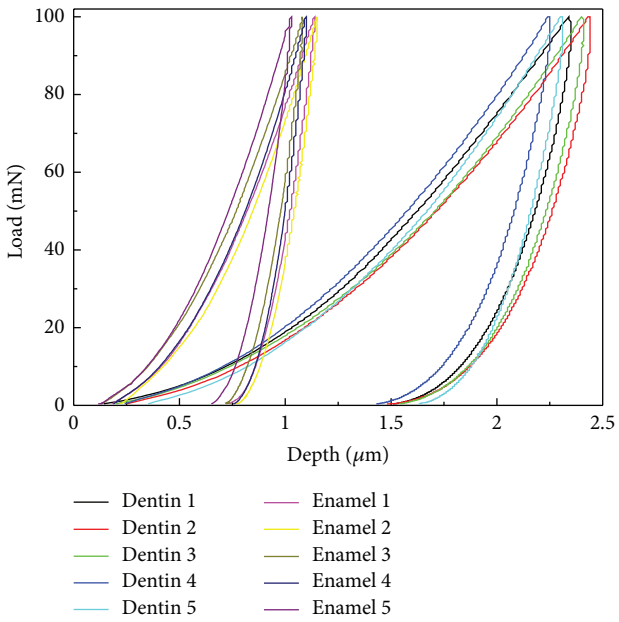

Figure 3: Typical load (P) versus depth (h) plots from the nanoindentation experiments on the enamel nanocomposite and dentin zones of human premolar teeth.

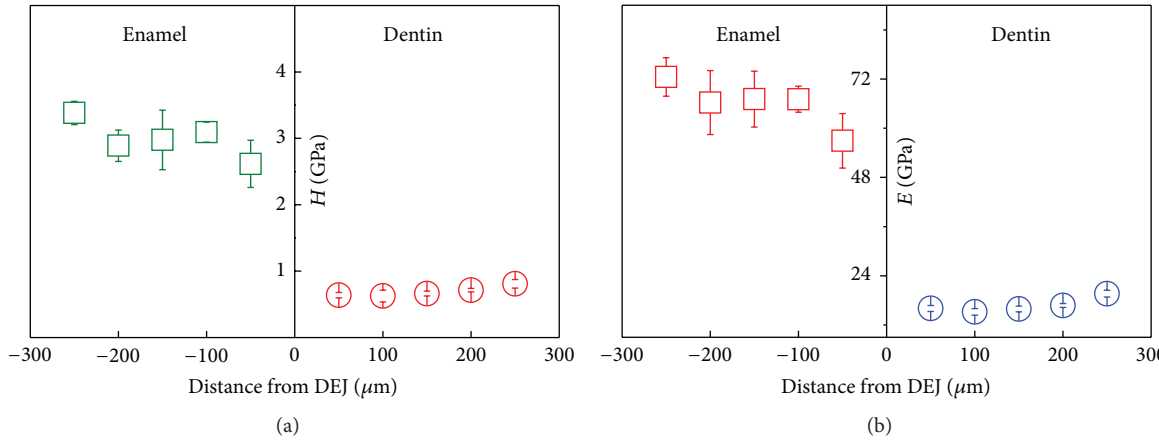

Figure 4: (a) Nanohardness and (b) Young's modulus of the enamel nanocomposite and dentin zones as a function of distance from the DEJ zone.

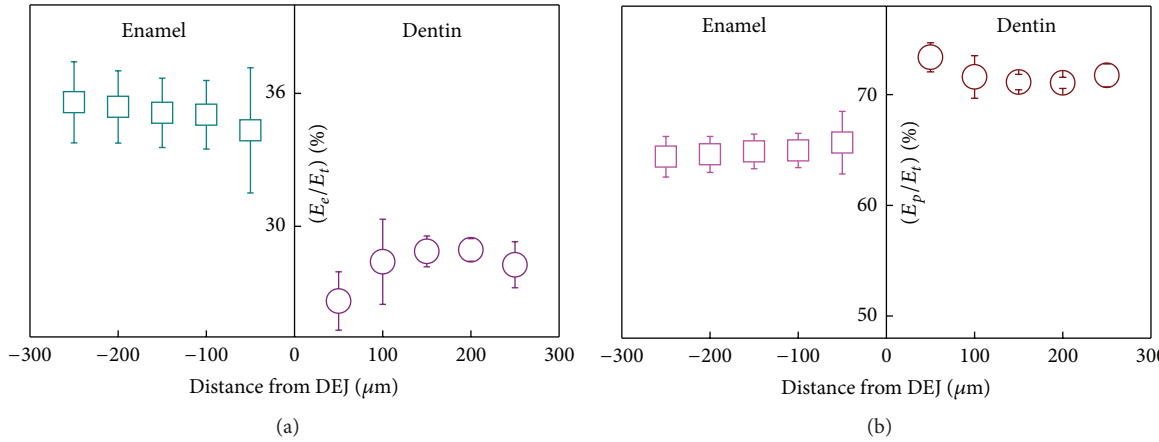

Figure 5: For the enamel nanocomposite and dentin zones, the percentage ratios of (a) elastic and (b) plastic to total energies of nanoindentation as a function of distance from the DEJ zone.

region. Thus, the experimental observations made in the present work were similar to the data reported in the literature [4, 25, 26].

The elastic recovery was much more in the enamel nanocomposite (Figure 5(a)) than in dentin region while the plastic deformation was much more in dentin (Figure 5(b)) than in the enamel nanocomposite region. The enamel nanocomposite region had undergone better degree of biomineralization as reflected in its relatively higher calcium content (Figure 6) as compared to that of the dentin region. Other workers [3] have also suggested that the better nanomechanical properties of the enamel nanocomposite region were linked to its higher degree of biomineralization in comparison to that of the dentin region.

The lower magnification SEM photomicrographs of the Vickers indentations in the enamel nanocomposite region, the dentin region, and the enamel nanocomposite region very close to DEJ are shown, respectively, in Figures 7(a), 7(c), and 7(e) while the corresponding higher magnification SEM photomicrographs are illustrated in Figures 7(b), 7(d), and 7(f), respectively. It may be noted that, as expected, there was no crack generation in the dentin region (Figures 7(c) and 7(d)) and hence $K_{IC(e)}$ of the dentin region could not be measured.

The FESEM image of the DEJ zone shows that the junction has got a very rough surface (Figure 8). The letters "E" and "D" in Figure 8 denote the enamel and the dentin regions adjacent to the junction. The $K_{IC(e)}$ was as low as 0.80 MPa·m$^{0.5}$ at middle enamel nanocomposite region but rose by about 40% to a magnitude of ~1.11 MPa·m$^{0.5}$ at a region in the immediate vicinity (e.g., within ~10 μm) of the DEJ zone (Figure 9). The experimentally measured $K_{IC(e)}$ data of the present work were comparable to the data reported in the literature [24, 25, 27, 30, 31, 34, 35].

Figure 10(a) shows the $K_{IC(e)}$ curves predicted by the Rule of Mixtures [19–21] as a function of the fracture toughness of the protein matrix phase (K_m) of the enamel nanocomposite. It may be noted from Figure 10(a) that the experimentally measured $K_{IC(e)}$ data (0.80 to 1.11 MPa·m$^{0.5}$, Figure 9) were between the predicted values of $K_{IC(e)}$ for which K_m had to

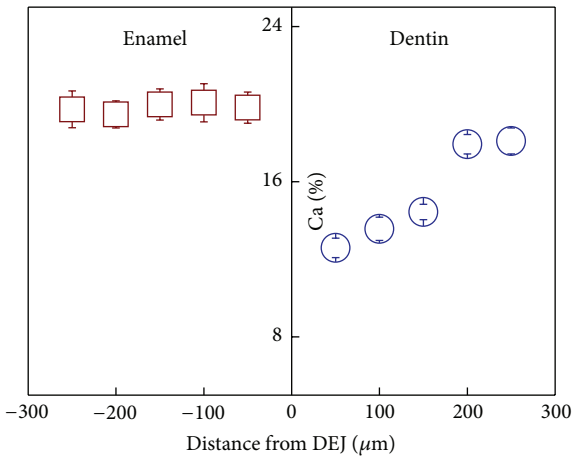

FIGURE 6: Variation of calcium percentages in the enamel nanocomposite and dentin zones as a function of distance from the DEJ zone.

be assumed to have a value lying in the range between 7 and 12 MPa·m$^{0.5}$. The Reuss and Angew [19] and the Voigt [20] models represent, respectively, the lower and upper bounds.

It may be noted further from the data presented in Figure 10(a) that the $K_{IC(e)}$ values predicted according to the Voigt model [20] were always greater than those predicted according to the Reuss model [19]. The data presented in Figure 10(b) shows the $K_{IC(e)}$ values predicted using the contiguity approach [42] as a function of the fracture toughness (K_m) of the protein matrix phase of the enamel nanocomposite.

4. Discussions

The SEM photomicrographs of the array of the nanoindents in the enamel nanocomposite and dentin portions around the DEJ did not show any obvious sign of cracking (Figure 2) because the load was ultralow. On a comparative scale a much higher amount of energy was absorbed during deformation at the nanoscale by the dentin (Figure 3) because it is a biopolymer that deforms in a viscoelastic manner, thereby dissipating more energy. Further, the slope of the unloading curve near its beginning was much stiffer in the enamel nanocomposite than in the dentin region, Figure 3. That is why Young's modulus of the enamel nanocomposite was much higher than that of the dentin region (Figure 4(b)). The enamel nanocomposite had higher nanohardness in comparison to that of the dentin region (Figure 4(a)) because the bioprotein matrix phase in it is reinforced by the nanocrystalline HAP rods. That is why the amount of energy spent in elastic deformation in the enamel nanocomposite (Figure 5(a)) was much more than that in dentin while the amount of energy spent in plastic deformation was much more in dentin than in the enamel nanocomposite, Figure 5(b). This picture also explains why the final depth of penetration in the enamel nanocomposite was much less than that in dentin at a comparable load (Figure 3). Hence, for the comparable ultralow load, the projected contact area in the enamel nanocomposite was much lesser than those in the dentin region. As a result, the nanohardness (H) of the enamel nanocomposite (Figure 4(a)) was much higher than those of the dentin regions. The other most important reason for the higher nanohardness of the enamel nanocomposite was the higher degree of biomineralization compared that of the dentin region (Figure 6). There is no contradiction at all between the results obtained in the present work and those reported earlier [12] where it was postulated that the lack of mineral phase content leads to the lower nanohardness of the enamel nanocomposite that was already hypomineralized. On the other hand, the present results rather confirm the prevalent views of other researchers [3, 12, 16] that the mechanical properties of the enamel nanocomposite are a strongly sensitive function of the extent of the mineral phase content, that is, the degree of biomineralization already undergone by the microstructure.

It is evident from the SEM photomicrographs presented in Figures 7(a) and 7(b) that for the applied load of 4.9 N all the four crack lengths associated with the typical Vickers microindentation impression did not necessarily have equal length and similar orientation with respect to the two major diagonals of the Vickers indent near the start of the middle enamel nanocomposite region. This information implies that even minor local microstructural variance can affect the crack length in the enamel nanocomposite.

The higher magnification view of the crack (Figure 7(b)) from the bottom of the [microindent] confirmed that the crack path was tortuous. The crack had suffered many minor deflections before getting arrested at the DEJ zone. On the other hand, only the Vickers indentation impression was visible in the dentin region (Figures 7(c) and 7(d)) when the experiment was conducted at the same load of 4.9 N.

However, the most interesting observation was that when the Vickers indentation at the same load of 4.9 N was conducted within ~10 μm of the DEJ region (Figure 7(e)), the crack lengths parallel to the DEJ zone were comparatively much longer in comparison to those perpendicular to the DEJ zone. Generally, the propagation of a crack from the bottom of the [microindent] across the DEJ zone was not observed (Figure 7(e)). These observations would suggest that the average crack length was much smaller near the DEJ zone than in the region near the start of the middle enamel nanocomposite. The very presence of a very rough yet rugged microstructural layer nearby, that is, the DEJ zone itself (Figure 8) also ensured that the crack did not cross over the DEJ zone. It is suggested, that as a result of all such contributions, the $K_{IC(e)}$ rose to about 1.11 MPa·m$^{0.5}$ at a region in the immediate vicinity (e.g., within ~10 μm) of the DEJ zone (Figure 9).

Further, near the DEJ zone, the magnitude of the factor $(E/H)^{0.5}$ in (1) was only 1% lower than that near the beginning of the middle enamel nanocomposite region while the magnitude of the factor $(P \cdot D^{-1.5})$ was ~60% higher near the DEJ zone in comparison to that near the beginning of the middle enamel nanocomposite region. This information provides an additional justification as to why the region very near DEJ zone was about 40% tougher than that of the region

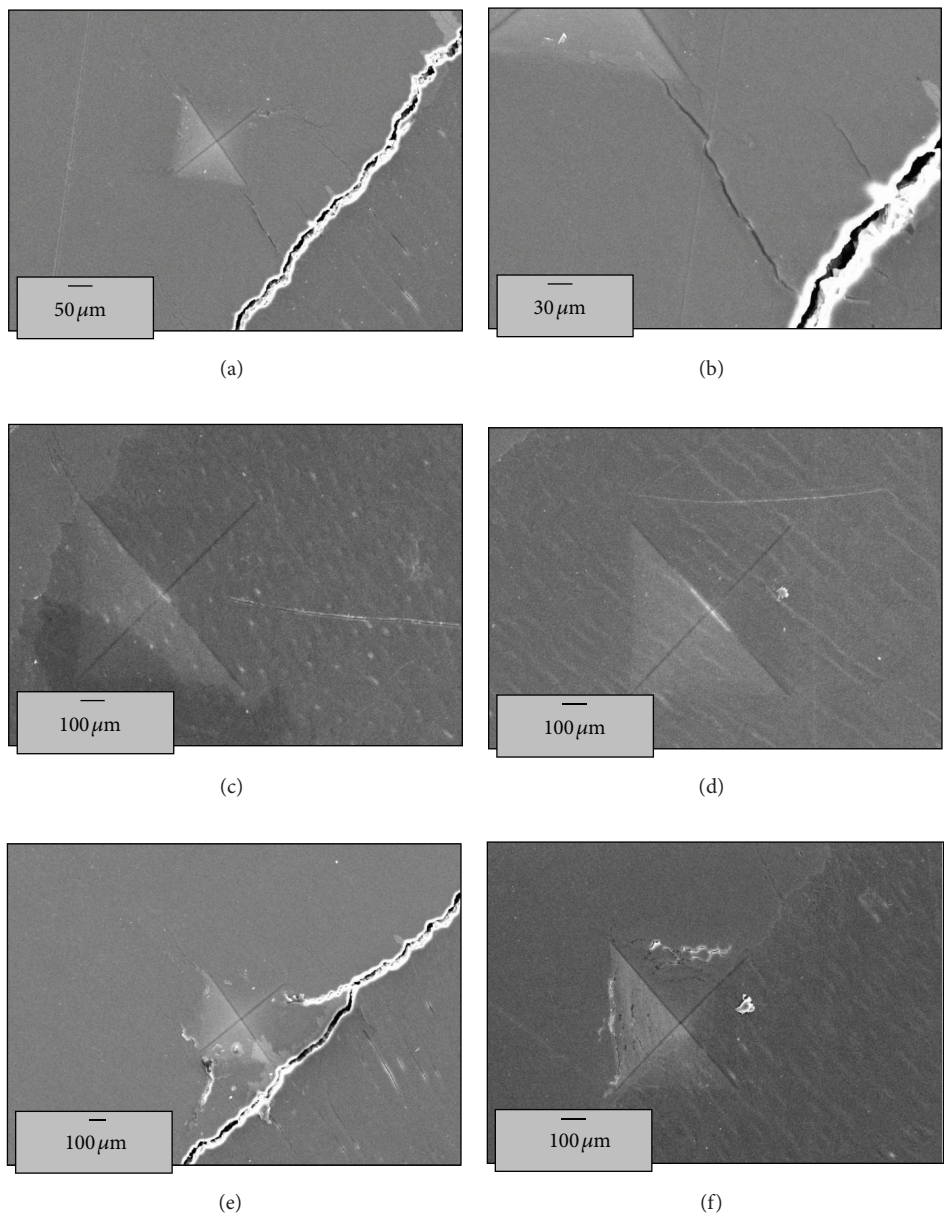

Figure 7: Typical SEM photomicrographs of (a) a Vickers indent at the enamel nanocomposite zone, (b) crack propagation near DEJ zone at higher magnification, (c) a Vickers indent at dentin zone very near to the DEJ zone, (d) a Vickers indent at dentin zone, (e) crack arrest for cracks from a Vickers indent very near to the DEJ zone, and (f) a Vickers indent at the DEJ zone.

near the starting of the middle enamel nanocomposite region. Microindentations made just at the DEJ zone showed that the cracks trying to propagate perpendicularly across the zone were arrested (Figure 7(f)) while those parallel to the interface could propagate parallel to the DEJ zone itself. This evidence confirms that the DEJ zone had a higher $K_{IC(e)}$. It happened because the microstructure of the DEJ zone was very rough as is evident from the FESEM photomicrograph (Figure 8). Thus, it may be concluded from the present experimental data that the region very near to the DEJ zone have $K_{IC(e)}$ much greater than those at the portion near the beginning of the middle enamel nanocomposite region.

The enamel nanocomposite was found to have an average $K_{IC(e)}$ of 0.88 MPa·m$^{0.5}$. It is well known that the enamel nanocomposite is a microscale-to-nanoscale hybrid nanocomposite with a hierarchical architecture [7–9]. As mentioned earlier, at a microscopic level, it consists of aligned hydroxyapatite microprisms surrounded by an organic sheath that plays the role of a protein matrix. At the nanoscale level, each prism contains numerous HAP nanocrystal rods separated by a nanometer-thin organic layer. The rod-like HAP crystals are oriented along the prism axis. In response to applied loading, the protein matrix shears to accommodate the strain due to the imposed deformation and transfers

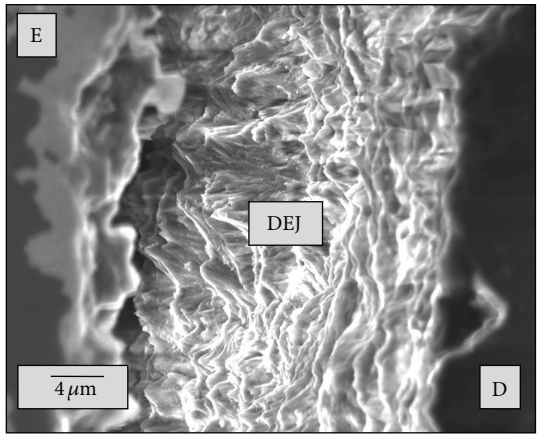

Figure 8: FESEM photomicrograph of the scalloped DEJ region.

load among the adjacent mineral components. This repetitive loading, load transfer followed by the subsequent loading process, may give rise to the observed pop-in effect (Figure 3) in the enamel nanocomposite during the present nanoindentation experiments.

The other two factors which may contribute are (a) the extent of local sharing of the total strain in between the protein matrix and the nanocrystalline HAP rods within the purview of the tension-shear-chain (TSC) model [43] and (b) the process of stretching of individual biomolecules in the bioprotein matrix. It is quite likely that each individual biomolecule contributes in an additive fashion locally to the complete stretching of the protein matrix layer.

Using micromechanics approach, the stiffness of a composite can be predicted. Most of the micromechanical models are derived from the need for predicting the elastic properties. However, other researchers have already established the link between the effective hardness values of a particle reinforced Ag-Ni composite and the hardness values of its constituent components by using the "Rule of Mixtures" approach [44]. In the present work, this approach was utilized to predict the $K_{\mathrm{IC(e)}}$ of the enamel nanocomposite. For making such prediction, an *adhoc* estimation of the K_m of the bioprotein matrix present in the enamel nanocomposite had to be made. Finally, the predicted data were compared with the experimentally measured toughness data.

The Reuss model [19] was used here to predict the longitudinal fracture toughness (K_1). In applying the Reuss model [19], it is implicitly assumed that the total amount of strain sustained by the reinforcing nanocrystalline HAP rods nearly equals that suffered by the bioprotein matrix phase. Thus, (K_1) is given by [19]

$$K_1 = K_h V_h + K_m V_m. \tag{2}$$

Similarly, the Voigt model predicts the longitudinal fracture toughness (K_2). In applying the Voigt model [20], it is implicitly assumed that the total amount of stress sustained by the reinforcing nanocrystalline HAP rods nearly equals that suffered by the bioprotein matrix phase. Thus, (K_2) is given by [20]

$$K_2 = \frac{K_h K_m}{\left(K_h V_m + K_m V_h\right)}. \tag{3}$$

In (2) and (3), K_h and K_m are the fracture toughness values of the reinforcing HAP nanocrystalline rods and the bioprotein matrix, and V_h and V_m are the volume fractions of the reinforcing HAP nanocrystalline rods and the biopolymer matrix.

In addition, the prediction of $K_{\mathrm{IC(e)}}$ was also done using the "Contiguity Model" [42]. In this model, a situation where the HAP nanocrystalline rods may or may not touch each other was taken care of by the factor "C" that denotes the degree of contiguity. For instance, $C = 0$ corresponds to a situation where the reinforcing HAP nanocrystalline rods are isolated and do not touch each other at all. Similarly, $C = 1$ corresponds to a situation where the reinforcing HAP nanocrystalline rods are all in perfect contact with each other. Thus, the fracture toughness (K_2) transverse to the direction of the orientation of the HAP nanocrystalline rods is given by [42]

$$K_2 = 2\left[1 - \nu_h + \left(\nu_h - \nu_m\right) V_m\right] \times \left[\begin{array}{l} (1 - C)\,\dfrac{B_h\left(2B_m + G_m\right) - G_m\left(B_h - B_m\right) V_m}{\left(2B_m + G_m\right) + 2\left(B_h - B_m\right) V_m} \\ +C\dfrac{B_h\left(2B_m + G_h\right) + G_h\left(B_m - B_h\right) V_m}{\left(2B_m + G_h\right) - 2\left(B_m - B_h\right) V_m} \end{array}\right], \tag{4}$$

where

$$B_h = \frac{E_h}{2\left(1 - \nu_h\right)}, \tag{5a}$$

$$B_m = \frac{E_m}{2\left(1 - \nu_m\right)}, \tag{5b}$$

$$G_h = \frac{E_h}{2\left(1 + \nu_h\right)}, \tag{5c}$$

$$G_m = \frac{E_m}{2\left(1 + \nu_m\right)}. \tag{5d}$$

Here, C lies between 0 and 1. Further, the quantities E_h, B_h, G_h, and ν_h represent, respectively, Young's modulus, bulk modulus, shear modulus, and Poisson's ratio of the reinforcing nanocrystalline HAP rods. Similarly E_m, B_m, G_m, and ν_m stand, respectively, for Young's modulus, bulk modulus, shear modulus, and Poisson's ratio of the bioprotein matrix in the enamel nanocomposite. The values for ν_h and ν_m were, respectively, taken to be 0.27 and 0.38 from the literature [45, 46].

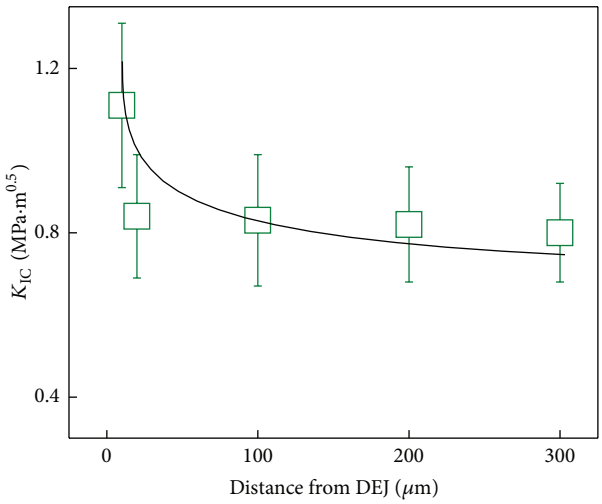

FIGURE 9: Variation of fracture toughness as a function of distance from the DEJ zone.

Similarly, the fracture toughness (K_1) values in a direction parallel to the orientation direction of the HAP nanocrystalline rods are given by the "modified rule of mixtures" as follows [42]:

$$K_1 = k\left(V_h K_h + V_m K_m\right), \tag{5}$$

where "k" ($0.9 < k < 1$) represents the degree of misalignment for the reinforcing HAP nanocrystalline rods.

The basis of the aforesaid "effective property" approach is embedded in the fact that the human dental enamel is a hybrid nanocomposite comprising the enamel prisms in an extracellular fluoride containing amelogenin protein matrix. The prisms themselves are composed of the HAP nanocrystalline rods (dia ~33–65 nm, length ~100–1000 nm) oriented along the c-axis [47]. The mature human enamel nanocomposite consists of more than 95% w/w of the mineral phase, 4-5% w/w water, and less than 1% of organic matter [48].

The experimental $K_{IC(e)}$ data of the nanocomposite was seen to be having a gradation, for example, it ranged from 1.11 ± 0.30 to 0.80 ± 0.10 MPa·m$^{0.5}$ (with an average value of about 0.88 ± 0.20 MPa·m$^{0.5}$) as we move from within ~10 μm of the DEJ zone up to a distance of 300 μm away from the DEJ zone. It is suggested that the fall in the $K_{IC(e)}$ values of the enamel nanocomposite (Figure 9) as we move from within ~10 μm of the DEJ zone up to a distance of ~300 μm away from the DEJ zone may be related to the localized smooth transition from one three-dimensional alignment of the HAP nanocrystalline rods to another [49]. Such localized microstructural and architectural transitions are characteristic of natural hierarchical biomaterials [49].

For the three values of V_h, that is, 0.92, 0.95, and 0.98, $K_{IC(e)}$ values were predicted as 1.12, 0.88, and 0.64 MPa·m$^{0.5}$ (Figure 10(a)) from the Voigt model [20]. Thus, the average predicted toughness was 0.88 ± 0.20 MPa·m$^{0.5}$ for $V_h \sim 0.92$ to 0.95. However, for the same values of V_h, the predicted values of toughness were 0.52, 0.50, and 0.49 MPa·m$^{0.5}$ (Figure 10(a)) from the Reuss model [19]. Thus, the average predicted toughness was 0.50 ± 0.01 MPa·m$^{0.5}$ for $V_h \sim 0.92$ to 0.95. According to both models, to predict the average experimental $K_{IC(e)}$ of the enamel nanocomposite, the fracture toughness for the protein matrix (K_m) had to be taken as ~8.5 MPa·m$^{0.5}$. In absence of the exact experimental data on the K_m of human dental enamel nanocomposite, it may be only mentioned that experimental data on K_{IC} of cattle horn sheath keratin was reported [50] to be of the same order as assumed here, for example, ~3.9 MPa·m$^{0.5}$.

It may be seen from the data of Figure 10(a) that the Voigt model [20] gave a reasonably close prediction to the experimental data while the Reuss model [19] absolutely underpredicted (Figure 10(a)) the experimental data of $K_{IC(e)}$. Similar conclusion was drawn also by other researchers [18] while attempting to predict Young's modulus of the protein matrix by using the Reuss and Angew [19] and the Voigt [20] models.

Using the contiguity approach [42] and assuming the K_m as ~8.5 MPa·m$^{0.5}$ with $k = 0.95$, the longitudinal fracture toughness (K_1) values of the enamel nanocomposite were predicted as ~1.14, 0.88, and 0.62 MPa·m$^{0.5}$ (Figure 10(b)) for the three values of V_h, that is, 0.92, 0.95, and 0.98, respectively. Thus, in this case also the average predicted toughness was 0.88 ± 0.30 MPa·m$^{0.5}$ for $V_h \sim 0.92$ to 0.95. In other words, the predicted average data matched nicely with the experimental $K_{IC(e)}$ data.

However, in the case of loading perpendicular to the orientation of the HAP nanocrystalline rods, assuming the K_m as ~8.5 MPa·m$^{0.5}$ for $C = 0$ (i.e., no contact between the HAP nanocrystalline rods) and $V_h = 0.92$, 0.95, and 0.98, the transverse fracture toughness (K_2) values were predicted as ~0.65, 0.59, and 0.52 MPa·m$^{0.5}$. Thus, the average predicted toughness was 0.59 ± 0.10 MPa·m$^{0.5}$ for $V_h \sim 0.92$ to 0.95. Similarly, for $C = 1$ (i.e., full contact along the length of the HAP nanocrystalline rods) and $V_h = 0.92$, 0.95, and 0.98, the $K_{IC(e)}$ values were predicted as ~0.53, 0.51, and 0.49 MPa·m$^{0.5}$, respectively (Figure 10(b)). Hence, the average predicted toughness was 0.51 ± 0.02 MPa·m$^{0.5}$ for $V_h \sim 0.92$ to 0.95. Both of these values (0.59 ± 0.1 and 0.51 ± 0.02 MPa·m$^{0.5}$) were unacceptably low with respect to the present experimental data on $K_{IC(e)}$ of the enamel nanocomposite. Therefore, it reveals the limitation of the contiguity approach as far as $K_{IC(e)}$ prediction is concerned.

Further, using the average experimental data of 0.88 MPa·m$^{0.5}$ for $K_{IC(e)}$, the work of fracture (γ) for the enamel nanocomposite was calculated using the following:

$$\gamma = \frac{\left(K_{IC(e)}\right)^2\left(1 - \nu_e{}^2\right)}{2E}, \tag{6}$$

where ν_e is Poisson's ratio (~0.28) of enamel nanocomposite [33] and the other terms are already explained. Thus, the work of fracture (γ) was estimated to be ~7 J·m^{-2} which was of the order of data (~13 J·m^{-2}) reported in the literature [49], thereby suggesting that the average experimental value of 0.88 MPa·m$^{0.5}$ for $K_{IC(e)}$ of the enamel nanocomposite was reasonable.

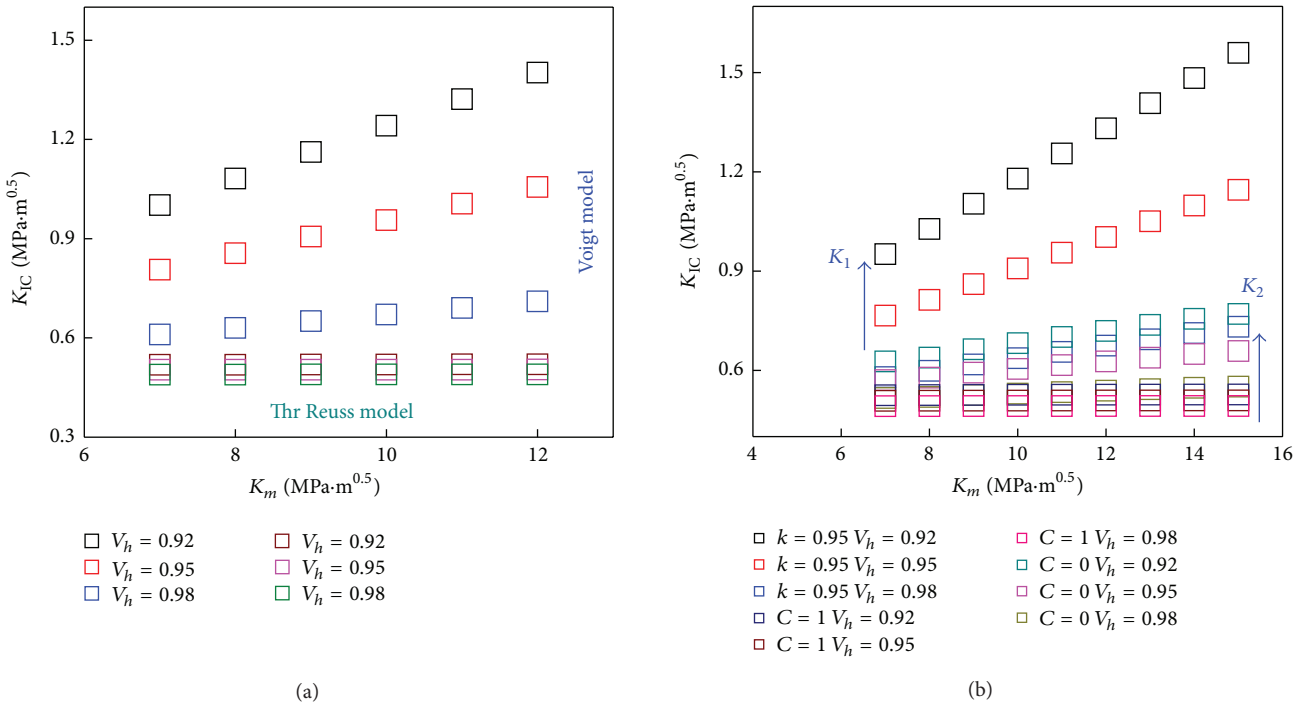

FIGURE 10: Prediction of fracture toughness of the human premolar dental enamel nanocomposite by (a) the "Rule of Mixtures" and (b) the "Contiguity Approach."

5. Conclusion

The major conclusions from the present work are the following.

(a) To the best of our knowledge, here we report possibly for the very first time a simultaneous evaluation of the nanohardness (H), Young's modulus (E), and $K_{IC(e)}$ in the vicinity of the DEJ zone for adult Indian premolar teeth. Both nanohardness (H) and Young's modulus (E) were evaluated by the nanoindentation technique using a Berkovich indenter at a load of 100 mN while the $K_{IC(e)}$ from near the middle to inner enamel nanocomposite region extending up to within ~10 μm of the DEJ zone was evaluated by microindentation technique with a Vickers indenter at a load of 4.9 N.

(b) Depending on the location, the average nanohardness (H), for example, 2–4 GPa, and Young's moduli (E), for example, 50–70 GPa of the enamel nanocomposite region, were much higher than those (H < 1 GPa, E < 25 GPa) of the dentin region. The $K_{IC(e)}$ was low at ~0.80 MPa·m$^{0.5}$ at the beginning of the middle enamel nanocomposite region but increased by ~40% to ~1.11 MPa·m$^{0.5}$ within ~10 μm of the DEJ zone.

(c) Prediction of the $K_{IC(e)}$ data was done by using the Voigt model, the Reuss model, and contiguity approach. Following the Voigt model and assuming the fracture toughness for the bioprotein matrix (K_m) phase to be ~8.5 MPa·m$^{0.5}$, the predicted data matched well with the average experimental data because the stress in the reinforcing nanocrystalline HAP rods phase was nearly equal to that in the bioprotein matrix phase. However, in the case of loading perpendicular to the orientation of the HAP nanocrystalline rods, both the Reuss model and the contiguity model with or without physical contact between the HAP nanocrystalline rods underpredict the experimental data. Nevertheless the modified Rule of Mixture with a misalignment factor (k) ~0.95 for the reinforcing nanocrystalline HAP rods also could predict $K_{IC(e)}$ data with reasonable accuracy.

Acknowledgments

The authors (N. Biswas and A. K. Mukhopadhyay) are thankful to the Director, of the Central Glass and Ceramic Research Institute (CGCRI), Kolkata, for his kind permission to publish this paper. In addition, the authors are grateful for the infrastructural support received from all colleagues and particularly those received from the colleagues of the Mechanical Property Evaluation Section at CGCRI. Finally, the authors gratefully acknowledge the financial support received from CSIR (Network Project TAREMaC no: NWP 0027). B_h, G_h, and ν_h represent, respectively,

References

[1] S. N. Bhaskar, *Orban's Oral Histology and Embryology*, Harcourt Brace and Company, Singapore, 11th edition, 1999.

[2] V. Imbeni, J. J. Kruzic, G. W. Marshall, S. J. Marshall, and R. O. Ritchie, "The dentin-enamel junction and the fracture of human teeth," *Nature Materials*, vol. 4, no. 3, pp. 229–232, 2005.

[3] L. H. He and M. V. Swain, "Enamel-A functionally graded natural coating," *Journal of Dentistry*, vol. 37, no. 8, pp. 596–603, 2009.

[4] Y. L. Chan, A. H. W. Ngan, and N. M. King, "Nano-scale structure and mechanical properties of the human dentine-enamel junction," *Journal of the Mechanical Behavior of Biomedical Materials*, vol. 4, no. 5, pp. 785–795, 2011.

[5] S. Marwan, A. Haik, A. Trinkle, D. Garcia, and F. Yang, "Investigation of the nanomechanical and tribological properties of dental materials," *International Journal of Theoretical and Applied Multiscale Mechanics*, vol. 1, no. 1, pp. 1–15, 2009.

[6] S. F. Ang, E. L. Bortel, M. V. Swain, A. Klocke, and G. A. Schneider, "Size-dependent elastic/inelastic behavior of enamel over millimeter and nanometer length scales," *Biomaterials*, vol. 31, no. 7, pp. 1955–1963, 2010.

[7] F. Lippert, D. M. Parker, and K. D. Jandt, "Susceptibility of deciduous and permanent enamel to dietary acid-induced erosion studied with atomic force microscopy nanoindentation," *European Journal of Oral Sciences*, vol. 112, no. 1, pp. 61–66, 2004.

[8] J. Ge, F. Z. Cui, X. M. Wang, and H. L. Feng, "Property variations in the prism and the organic sheath within enamel by nanoindentation," *Biomaterials*, vol. 26, no. 16, pp. 3333–3339, 2005.

[9] L. Angker, M. V. Swain, and N. Kilpatrick, "Micro-mechanical characterisation of the properties of primary tooth dentine," *Journal of Dentistry*, vol. 31, no. 4, pp. 261–267, 2003.

[10] J. Zhou and L. L. Hsiung, "Depth-dependent mechanical properties of enamel by nanoindentation," *Journal of Biomedical Materials Research A*, vol. 81, no. 1, pp. 66–74, 2007.

[11] I. R. Spears, "A three-dimensional finite element model of prismatic enamel: a re-appraisal of the data on the young's modulus of enamel," *Journal of Dental Research*, vol. 76, no. 10, pp. 1690–1697, 1997.

[12] Z. H. Xie, E. K. Mahoney, N. M. Kilpatrick, M. V. Swain, and M. Hoffman, "On the structure-property relationship of sound and hypomineralized enamel," *Acta Biomaterialia*, vol. 3, no. 6, pp. 865–872, 2007.

[13] Z. Xie, M. Swain, P. Munroe, and M. Hoffman, "On the critical parameters that regulate the deformation behaviour of tooth enamel," *Biomaterials*, vol. 29, no. 17, pp. 2697–2703, 2008.

[14] F. R. Reich, B. B. Brenden, and N. S. Porter, *Ultrasonic Imaging of Teeth*, Batelle Memorial Institue, Washington, DC, USA, 1967.

[15] M. Staines, W. H. Robinson, and J. A. A. Hood, "Spherical indentation of tooth enamel," *Journal of Materials Science*, vol. 16, no. 9, pp. 2551–2556, 1981.

[16] R. Rohanizadeh, F. S. M. Ismail, N. M. Kilpatrick, M. V. Swain, and E. K. Mahoney, "Mechanical properties and microstructure of hypomineralised enamel of permanent teeth," *Biomaterials*, vol. 25, no. 20, pp. 5091–5100, 2004.

[17] L. H. He, N. Fujisawa, and M. V. Swain, "Elastic modulus and stress-strain response of human enamel by nano-indentation," *Biomaterials*, vol. 27, no. 24, pp. 4388–4398, 2006.

[18] J. Zhou and L. L. Hsiung, "Biomolecular origin of the rate-dependent deformation of prismatic enamel," *Applied Physics Letters*, vol. 89, no. 5, pp. 051904(1)–051904(3), 2006.

[19] A. Reuss and Z. Angew, "Berechnung der Flie grenze von Mischkristallen auf Grund der Plastizit tsbedingung für Einkristalle," *ZAMM- Journal of Applied Mathematics and Mechanics*, vol. 9, pp. 49–58, 1929.

[20] W. Voigt, "Uber die Beziehung zwischen den beiden Elastiziitatskonstanten isotroper Korper," *Philosophical Transactions*, vol. 38, pp. 573–587, 1889.

[21] R. Hill, "The elastic behaviour of a crystalline aggregate," *Proceedings of the Physical Society A*, vol. 65, no. 5, pp. 349–354, 1952.

[22] R. G. Craig, F. A. Peyton, and D. W. Johnson, "Compressive properties of enamel dental cements and gold," *Journal of Dental Research*, vol. 40, no. 5, pp. 936–945, 1961.

[23] S. T. Rasmussen, R. E. Patchin, D. B. Scott, and A. H. Heuer, "Fracture properties of human enamel and dentin," *Journal of Dental Research*, vol. 55, no. 1, pp. 154–164, 1976.

[24] R. Hassan, A. A. Caputo, and R. F. Bunshah, "Fracture toughness of human enamel," *Journal of Dental Research*, vol. 60, no. 4, pp. 820–827, 1981.

[25] H. H. K. Xu, D. T. Smith, S. Jahanmir et al., "Indentation damage and mechanical properties of human enamel and dentin," *Journal of Dental Research*, vol. 77, no. 3, pp. 472–480, 1998.

[26] H. Fong, M. Sarikaya, S. N. White, and M. L. Snead, "Nano-mechanical properties profiles across dentin-enamel junction of human incisor teeth," *Materials Science and Engineering C*, vol. 7, no. 2, pp. 119–128, 2000.

[27] S. N. White, W. Luo, M. L. Paine, H. Fong, M. Sarikaya, and M. L. Snead, "Biological organization of hydroxyapatite crystallites into a fibrous continuum toughens and controls anisotropy in human enamel," *Journal of Dental Research*, vol. 80, no. 1, pp. 321–326, 2001.

[28] L. H. He and M. V. Swain, "Contact induced deformation of enamel," *Applied Physics Letters*, vol. 90, no. 17, pp. 171916(1)–171916(3), 2007.

[29] S. Park, D. H. Wang, D. Zhang, E. Romberg, and D. Arola, "Mechanical properties of human enamel as a function of age and location in the tooth," *Journal of Materials Science*, vol. 19, no. 6, pp. 2317–2324, 2008.

[30] S. Park, J. B. Quinn, E. Romberg, and D. Arola, "On the brittleness of enamel and selected dental materials," *Dental Materials*, vol. 24, no. 11, pp. 1477–1485, 2008.

[31] D. Bajaj, A. Nazari, N. Eidelman, and D. D. Arola, "A comparison of fatigue crack growth in human enamel and hydroxyapatite," *Biomaterials*, vol. 29, no. 36, pp. 4847–4854, 2008.

[32] S. Roy and B. Basu, "Mechanical and tribological characterization of human tooth," *Materials Characterization*, vol. 59, no. 6, pp. 747–756, 2008.

[33] S. F. Ang, T. Scholz, A. Klocke, and G. A. Schneider, "Determination of the elastic/plastic transition of human enamel by nanoindentation," *Dental Materials*, vol. 25, no. 11, pp. 1403–1410, 2009.

[34] D. Bajaj and D. Arola, "Role of prism decussation on fatigue crack growth and fracture of human enamel," *Acta Biomaterialia*, vol. 5, no. 8, pp. 3045–3056, 2009.

[35] S. K. Padmanabhan, A. Balakrishnan, M. C. Chu, T. N. Kim, and S. J. Cho, "Micro-indentation fracture behavior of human enamel," *Dental Materials*, vol. 26, no. 1, pp. 100–104, 2010.

[36] Y. R. Jeng, T. T. Lin, H. M. Hsu, H. J. Chang, and D. B. Shieh, "Human enamel rod presents anisotropic nanotribological properties," *Journal of the Mechanical Behavior of Biomedical Materials*, vol. 4, no. 4, pp. 515–522, 2011.

[37] S. N. White, V. G. Miklus, P. P. Chang et al., "Controlled failure mechanisms toughen the dentino-enamel junction zone," *Journal of Prosthetic Dentistry*, vol. 94, no. 4, pp. 330–335, 2005.

[38] X. D. Dong and N. D. Ruse, "Fatigue crack propagation path across the dentinoenamel junction complex in human teeth," *Journal of Biomedical Materials Research A*, vol. 66, no. 1, pp. 103–109, 2003.

[39] V. Imbeni, J. J. Kruzic, G. W. Marshall, S. J. Marshall, and R. O. Ritchie, "The dentin-enamel junction and the fracture of human teeth," *Nature Materials*, vol. 4, no. 3, pp. 229–232, 2005.

[40] W. C. Oliver and G. M. Pharr, "Improved technique for determining hardness and elastic modulus using load and displacement sensing indentation experiments," *Journal of Materials Research*, vol. 7, no. 6, pp. 1564–1580, 1992.

[41] G. R. Anstis, P. Chantikul, B. R. Lawn, and D. B. Marshall, "A critical evaluation of indentation techniques for measuring fracture toughness: I, direct crack measurements," *Journal of the American Ceramic Society*, vol. 64, no. 9, pp. 533–538, 1981.

[42] S. W. Tsai, "Structural behavior of composites materials," 1964, NSA-CR-71.

[43] H. Gao, B. Ji, I. L. Jäger, E. Arzt, and P. Fratzl, "Materials become insensitive to flaws at nanoscale: lessons from nature," *Proceedings of the National Academy of Sciences of the United States of America*, vol. 100, no. 10, pp. 5597–5600, 2003.

[44] H. S. Kim, "On the rule of mixtures for the hardness of particle reinforced composites," *Materials Science and Engineering A*, vol. 289, no. 1-2, pp. 30–33, 2000.

[45] J. B. Park and R. S. Lakes, *BioMaterials: An Introduction, in Ceramic Implant Materials, 1979*, Plenum Press, New York, Ny, USA, 1992.

[46] A. Franck, G. Cocquyt, P. Simoens, and N. De Belie, "Biomechanical properties of Bovine claw horn," *Biosystems Engineering*, vol. 93, no. 4, pp. 459–467, 2006.

[47] C. Robinson, J. Kirkham, and R. C. Shore, *Dental Enamel Formation to Destruction*, CRC Press, Boca Raton, Fla, USA, 1995.

[48] Y. W. Fan, Z. Sun, R. Wang, C. Abbott, and J. Moradian-Oldak, "Enamel inspired nanocomposite fabrication through amelogenin supramolecular assembly," *Biomaterials*, vol. 28, no. 19, pp. 3034–3042, 2007.

[49] J. McKittrick, P. Y. Chen, L. Tombolato et al., "Energy absorbent natural materials and bioinspired design strategies: a review," *Materials Science and Engineering C*, vol. 30, no. 3, pp. 331–342, 2010.

[50] B. W. Li, H. P. Zhao, X. Q. Feng, W. W. Guo, and S. C. Shan, "Experimental study on the mechanical properties of the horn sheaths from cattle," *Journal of Experimental Biology*, vol. 213, no. 3, pp. 479–486, 2010.